ACS APPLIED MATERIALS & INTERFACES

www.acsami.org

Research Article

Realizing Optoelectronic Devices from Crumpled Two-Dimensional Material Heterostructures

M. Abir Hossain, Jaehyung Yu, and Arend M. van der Zande*

Cite This: https://dx.doi.org/10.1021/acsami.0c10787

Read Online

ACCESS | Metrics & More | Article Recommendations | Supporting Information

ABSTRACT: Due to their high in-plane stiffness and low flexural rigidity, two-dimensional (2D) materials are excellent candidates for engineering three-dimensional (3D) nanostructures using crumpling. An important new direction is to integrate 2D materials into crumpled heterostructures, which can have much more complex device geometries. Here, we demonstrate phototransistors from crumpled 2D heterostructures formed from graphene contacts to a monolayer transition-metal dichalcogenide (MoS_2, WSe_2) channel and quantify the membrane morphology and optoelectronic performance. First, we examined the morphology of folds in the heterostructure and constituent monolayers under uniaxial compression. The 2D membranes relieve the stress by delaminating from the substrate and creating nearly periodic folds whose spacing depends on the membrane type. The matched mechanical stiffness of the constituting layers allows the 2D heterostructure to maintain a conformal interface through large deformations. Next, we examined the optoelectronic performance of a biaxially crumpled graphene–WSe_2 phototransistor. Photoluminescence (PL) spectroscopy shows that the optical band gap of WSe_2 shifts by less than 2 meV between flat and 15% biaxial crumpling, corresponding to a change in strain of less than 0.05%. The photoresponsivity scaled as $P^{-0.38}$ and reached 20 A/W under an illumination power density of 4 μW/cm^2 at 20 V bias, a performance comparable to flat photosensors. Using photocurrent microscopy, we observe that the photoresponsivity increases by only 20% after crumpling. Both the PL and photoresponse confirm that crumpling and delamination prevent the buildup of compressive strain leading to highly deformed materials and devices with similar performance to their flat analogs. These results set a foundation for crumpled all-2D heterostructure devices and circuitry for flexible and stretchable electronic applications.

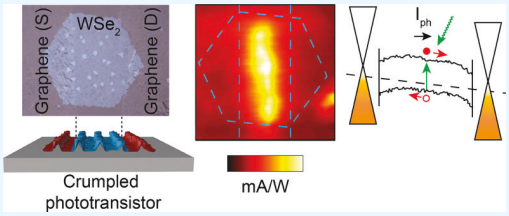

KEYWORDS: *2D materials, heterostructures, photodetector, stretchable, crumpled*

INTRODUCTION

The increasing demand for wearable technologies requires materials capable of undergoing large mechanical deformations yet maintaining electronic properties rivaling the conventional materials used in rigid electronics. Great progress has been made in demonstrating functional deformable devices from patterned delamination of stiff thin films[1] or from soft organic molecules.[1−3] However, in most materials, there is a fundamental tradeoff between mechanical pliability and electronic mobility, limiting both device size and performance. Conventional semiconductors become unstable in films <10 nm thick, while soft materials and organic electronics are pliable but suffer from low mobility.[2] Atomic membranes from two-dimensional (2D) materials are naturally stable down to a monolayer and thus offer a notable exception to this tradeoff. They are the strongest materials in the world (Young's modulus up to 1000 GPa) yet are as pliable as a cell membrane (bending modulus ∼1−10 eV).[4,5] Simultaneously, they are electronically active, with different members offering a pallet of electronic properties including metals, semiconductors, and insulators. By stacking monolayers of different 2D materials, it is possible to engineer nearly any electronic component with nanometer-scale dimensions[6,7] and tailor the emergent quantum phenomena.[8−10] Combining these insights reveals that 2D materials are ideal for applications combining mechanics with electronics such as resonant membranes in nanoelectromechanical systems,[11−13] flat strained layers on bent substrates for flexible electronics,[14−17] and active layers for stretchable electronics.[18,19]

The goal of this work is to explore the potential for an emerging class of deformed electronics based on crumpled 2D materials and specifically van der Waals heterostructures. In order to be deformed beyond a few percent, 2D materials must first be crumpled[19−21] so that the out-of-plane deformation relieves the in-plane stresses. The highly deformed surfaces of crumpled 2D materials lead to applications in wearable electronics,[22−24] supercapacitors,[25] multifunctional surfaces,[26] and sensors.[18,27] All these applications utilize single 2D materials, often integrating them with conventional thin films

Received: June 13, 2020
Accepted: September 25, 2020
Published: September 25, 2020

to achieve a full device functionality,[18,23,28] which are brittle and far stiffer than the 2D materials. To fully realize the potential of 2D materials for deformable electronics, it is necessary to move to all-2D heterostructures. In 2D material multilayers, slip at the van der Waals interface acts to relieve strain,[29] leading to structures and devices orders of magnitude more deformable than conventional thin films.

Here, we demonstrate phototransistors from crumpled transition-metal dichalcogenide (TMDC)−graphene van der Waals heterostructures where graphene acts as an electrode and the TMDC acts as a channel. By applying uniaxial or biaxial compressive strain, we induced 3D crumples or folds in the 2D membrane. We investigated the mechanics by measuring the relative morphology of the crumpled heterostructure and constituent monolayers and the optoelectronic properties of the resulting devices. The ability of 2D heterostructures to take up large strain through conformal crumpling without strongly affecting the photoresponse demonstrates potential for deformable electronics. While here we focus on only one device demonstration, the insights and method can be applied to hundreds of device concepts from 2D heterostructures, opening up possibilities for crumpled circuitry from all-2D materials.

EXPERIMENTAL SECTION

Figure 1a illustrates the uniaxial and biaxial crumpling of a 2D heterostructure on a prestrained substrate. Figure 1b shows the optical images of a MoS_2−graphene heterostructure before and after crumpling. The heterostructure consists of two patterned monolayer graphene sheets separated by 20 μm, which are aligned and transferred onto isolated islands of monolayer TMDCs including MoS_2 (shown in Figure 1) or WSe_2 (shown in Figure S1). The layers are offset from each other, so the heterostructure functions as an in-plane phototransistor with graphene operating as contacts to the TMDC channel. Shown in Figure S2, the monolayer structure of these materials is confirmed with Raman and photoluminescence spectroscopy. We fabricated the entire heterostructure on a uniaxially or biaxially prestrained elastomer substrate, either polydimethylsiloxane (PDMS) or VHB (3M Inc.), loaded into a custom-built holder (Figure S3), and then released the prestrain to induce compression and crumpling in the material. Step-by-step details about the growth, fabrication, and transfer process for all the structures are provided in Sections S1 and S2.

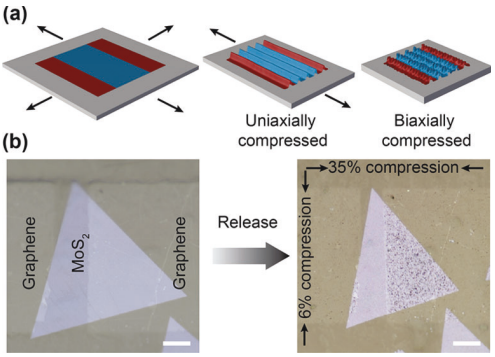

Figure 1. Crumpled TMDC−graphene heterostructure for sensing application. (a) Schematic illustration of the crumpling process of a 2D heterostructure on a biaxially prestrained substrate showing both uniaxial and biaxial crumpled structures. (b) Optical image of a MoS_2 phototransistor with graphene electrodes before and after crumpling. The scale bar is 20 μm.

RESULTS AND DISCUSSION

In Figure 2, we compare the relative morphology of the offset MoS_2−graphene heterostructure and constituent monolayers under uniaxial compression. Figure 2a schematically shows the relative morphology of folds in the different regions of the heterostructure. Figure 2b−d shows representative atomic force microscopy (AFM) topographic images from the three constituent regions in a single offset MoS_2−graphene heterostructure on PDMS under 7.5% uniaxial compression: (b) MoS_2−graphene heterostructure (blue-red), (c) monolayer MoS_2 (blue), and (d) monolayer graphene (red). In the heterostructure, MoS_2 is at the top, and graphene is at the bottom, in contact with the substrate. The advantage of using the offset heterostructure geometry is that it enables direct comparison of the relative morphology of each region under the same compression, substrate, processing, and measurement conditions. As seen in all images, the 2D material delaminates from the surface leading to the creation of nearly periodic hairpin folds. However, each region shows a different spacing of the folds. In addition, we observe cracks perpendicular to the folds. As shown in Figure S4, the Poisson ratio of the substrate leads to cracking in uniaxially compressed but not biaxially compressed samples.[30,31] For this study, we choose uniaxial compression because biaxial compression leads to complex fractal crumpled structures[18,19,25,26] while uniaxial compression leads to delamination of the 2D material from the substrate and the creation of nearly periodic hairpin folds[21,32−35] that are easier to image and quantify.[21] Two different substrates were used in this study: PDMS and VHB. There are three critical differences between the two substrates: stretchability, adhesive strength, and surface roughness. PDMS is relatively flat, with low adhesion, but has low stretchability, while VHB may be stretched by up to 300%, with higher adhesion and larger surface roughness. We chose to use a PDMS substrate for morphology analysis to allow direct comparison with previous measurements of 2D monolayers[21] and a VHB substrate for phototransistor fabrication for potential stretchable applications.

In Figure 2e, we compare the average spacing of the folds for each of the three different regions. In order to extract the fold spacing, we applied peak tracking to measure the positions of each of the folds in the AFM images and calculated the average spacing between them. The average fold spacing for each structure was $L_{MoS_2} = 1100 \pm 261$ nm, $L_{graphene} = 405 \pm 47$ nm, and $L_{MoS_2/graphene} = 650 \pm 82$ nm. In all membranes, the average period is determined by the mechanical moduli and the effective interfacial interactions with the substrate, which will be material- and substrate-dependent.[21] The error bars are the variation in spacing within each region. Delamination and fold generation are mechanical instabilities, so the precise point of fold generation will be affected by nanoscale inhomogeneities, like concentrations of stress at edges, shape of the compressed 2D membrane, particles at the interface, and surface roughness. As a comparison, the monolayer MoS_2 results agree with previous work that showed a fold spacing of 1100 nm corresponding to an applied compressive strain of 8%.[21] In contrast, the fold spacing for CVD-grown monolayer graphene is much smaller than previous measurements on exfoliated monolayer graphene, by a factor of ~4.[21] Because the Young's modulus should be similar, the lower period is representative of decreased substrate interactions and a lower adhesion. This lower interaction is consistent with observa-

https://dx.doi.org/10.1021/acsami.0c10787
ACS Appl. Mater. Interfaces XXXX, XXX, XXX−XXX

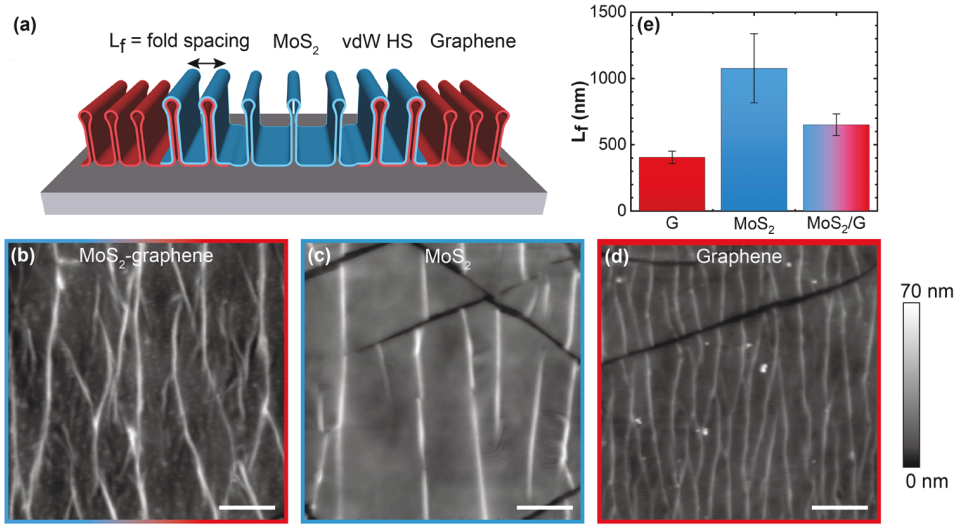

Figure 2. Morphology of an offset MoS_2−graphene heterostructure on PDMS under uniaxial compression. (a) Schematic of the nearly periodic fold generation in the heterostructure. The key feature is the variation in fold spacing of the different regions. (b−d) AFM topographic images from each region in the heterostructure at 7.5% compression. Each image is color coded by the corresponding region shown in panel (a). (b) MoS_2−graphene heterostructure, (c) MoS_2, (d) graphene. All scale bars are 1 μm. (e) Average fold spacing in different regions of the heterostructure at 7.5% compression.

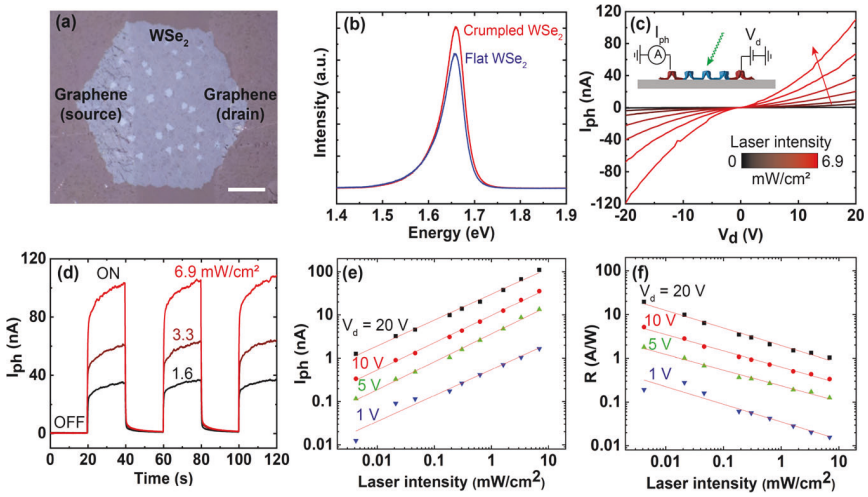

Figure 3. Photoresponse of a crumpled heterostructure phototransistor under global illumination. (a) Optical image of the 15% biaxially crumpled graphene−WSe_2 phototransistor. The scale bar is 10 μm. (b) Photoluminescence spectra of the monolayer WSe_2 before and after crumpling by 15%. (c) Photocurrent versus drain bias voltage under varying laser intensity. The inset shows the device configuration. (d) Dynamic photoresponse while switching the laser on and off, at three different laser intensities. The drain bias voltage is 20 V. (e,f) Photocurrent and photoresponsivity, respectively, versus laser intensity under different drain bias voltages. The photocurrent scales with intensity as $P^{0.62}$, while photoresponsivity scales as $P^{-0.38}$.

tions that CVD-grown graphene is much rougher and more contaminated than exfoliated graphene due to being grown on a rough copper substrate and the additional processing required for patterning and transfer.

The fold spacing of the heterostructure is between the fold spacing of the constituent graphene (shorter, bottom layer) and MoS_2 (longer, top layer). There are also additional bubbles between the folds, which are a common feature of heterostructures, and indicate good adhesion at the interface between layers.[36,37] Nonetheless, the smaller spacing of the heterostructure versus the monolayer MoS_2 (top layer) leads to the following important qualitative conclusions. First, both layers are delaminating together rather than the top layer delaminating from the bottom layer. Second, the bottom layer plays a more important role than the top layer in determining the spacing of folds in the heterostructure. These conclusions are supported by previous studies showing that 2D materials have stronger adhesion to each other than to rough substrates.[35,37−41] Third, the larger spacing of folds in the heterostructure versus monolayer graphene in the underlying layer means that the top layer contributes to the stiffness of the membrane. This conclusion is supported by nanoindentation experiments on graphene−MoS_2 heterostructures, which showed a residual friction between layers leading to a higher effective Young's modulus.[42] We adapted models on bending and folding of 2D materials and heterostructures to model the mechanics of the multiple interfaces but found that the bubbles at the interface and the roughness in the CVD-grown graphene

https://dx.doi.org/10.1021/acsami.0c10787
ACS Appl. Mater. Interfaces XXXX, XXX, XXX−XXX

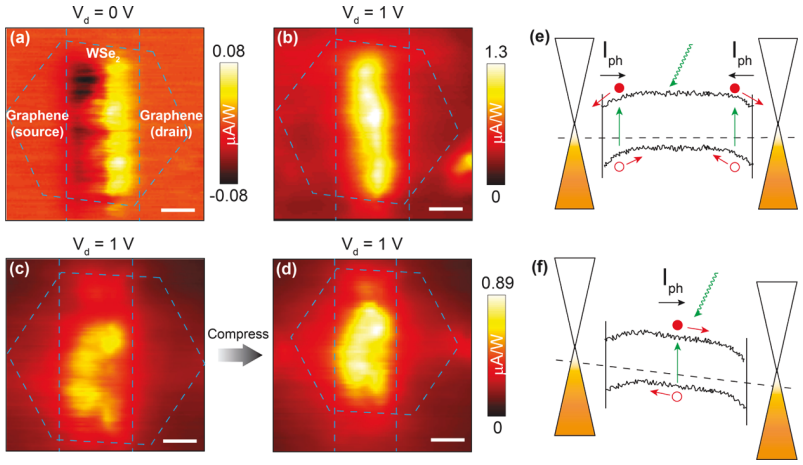

Figure 4. (a,b) Scanning photocurrent microscopy maps of the 15% biaxially crumpled graphene–WSe_2 phototransistor shown in Figure 3 for (a) zero drain bias and (b) 1 V drain bias. The positions of the graphene electrodes and WSe_2 channel are annotated on the maps. (c,d) Photocurrent maps of a second graphene–WSe_2 phototransistor under 1 V drain bias (c) before and (d) after crumpling under 15% biaxial compression. Laser power is 100 μW. The scale bar is 10 μm. (e,f) Band diagrams of the crumpled phototransistor corresponding to panels (a) and (b), respectively.

make quantification of the interface mechanics challenging and not meaningful. Nonetheless, this result shows that the 2D layers remain conformal to each other through large deformation, indicating that the heterostructure should maintain good electronic performance under large compression. Shown in Figure S5, to investigate the effect of different material–substrate combinations on the crumple morphology, we also analyzed MoS_2 on VHB and WSe_2 on PDMS under the same compression. We found that all 2D-substrate combinations yielded similar wavelengths of folds.

Next, in Figures 3 and 4, we quantify the optical response of a crumpled phototransistor. Figure 3a shows an optical image of a 15% biaxially crumpled graphene–WSe_2 heterostructure on VHB, with graphene on top of WSe_2, used as the phototransistor. Figure 3b shows the photoluminescence (PL) spectra (532 nm excitation) of monolayer WSe_2 before and after crumpling. The PL peak energy has a shift of less than 2 meV between unstrained and under 15% substrate compression. In comparison, straining 2D materials on flat substrates[43−46] or suspended membranes[47] lead to large shifts of the optical transition, for example, 48 meV/% strain in monolayer WSe_2.[45] These strain induced shifts are also observed in micron scale multilayer delamination buckling[48] or controlled monolayer wrinkling where the material remains laminated on the substrate under compression.[28] The small peak shift measured here show that the crumpling induces <0.05% average strain in the 2D material. This agrees with the morphology data and demonstrates that the large out-of-plane deformations from crumpling and delamination of WSe_2 from the substrate prevent strain buildup under substrate compression. Additional optical characterization results of WSe_2, MoS_2, and graphene before and after the crumpling process are provided in Figure S6.

To characterize the photoresponse of the phototransistor, we used two measurement modes − global illumination and scanning photocurrent microscopy. First, to make electrical contacts, we used a probe station and directly placed the electrical probes on the patterned graphene pads. In global illumination, we measured the photoresponse using a 2 mm spot from a 520 nm diode laser, providing uniform light intensity over the ∼20 μm × 40 μm active area of the entire device. To investigate the local photoresponse in the phototransistor, we used scanning photocurrent microscopy (SPCM), wherein the laser is focused into a ∼1 μm spot and rastered over the device to produce a spatially resolved map of the photoresponse. Together, these techniques give the effective performance of the phototransistor and unravel the underlying electronic band diagrams defining the device behavior. The measurement setup is described and shown in Figure S7.

In Figure 3c–f, we characterize the global photoresponse of the crumpled phototransistor. Figure 3c shows the photocurrent versus drain voltage under global illumination for fixed laser intensities from no illumination (dark) up to 6.9 mW/cm^2. Here, photocurrent is defined as the dark current subtracted from the drain current under illumination. However, the dark current is very small, so photocurrent ≈ drain current. The photoconductivity of the phototransistor increases nonlinearly with the drain bias. Similar behavior occurs in graphene-contacted WS_2 photodetectors on a hard silicon oxide substrate[49] and indicates that the conductivity is limited by Schottky barriers at the graphene electrodes.[50] Figure 3d shows the dynamic photoresponse of the crumpled phototransistor as a function of time while turning the illumination on and off. For this measurement, drain bias voltage is fixed at 20 V, and we vary the laser intensity from 1.6 to 6.9 mW/cm^2. The device demonstrates switching behavior as photocurrent increases under illumination (ON state) and goes down under the dark condition (OFF state). Just as in previous studies on flat phototransistors, there is a fast switching on and off due to the photoconductive effect and a slow change in the photoresponse due to photodoping.[51,52]

Figure 3e,f shows the photocurrent and photoresponsivity, respectively, as a function of laser intensity at fixed drain voltages. The photocurrent versus laser intensity follows a power law relation $I_{ph} \propto P^{\alpha}$, while the photoresponsivity scales as $R \propto P^{\alpha-1}$, where P is the incident laser intensity and $\alpha = 0.62 \pm 0.02$. Because of this scaling law, the photoresponsivity increases at low laser intensity, reaching a maximum photoresponsivity of 20 A/W at 20 V bias with a laser intensity of 4 μW/cm^2. This value is large compared to the photoresponsivity observed in silicon-based photodetectors or organic photodetectors, which show a photoresponsivity on the order of ∼100 mA/W,[51] demonstrating the applicability of

https://dx.doi.org/10.1021/acsami.0c10787
ACS Appl. Mater. Interfaces XXXX, XXX, XXX−XXX

the crumpled 2D heterostructure devices as highly sensitive photodetectors. While the crumpled heterostructure phototransistor is a novel structure, flat phototransistors from TMDCs are well studied in the literature and show a huge range of photoresponsivities (10^{-3} to 10^{5} A/W)[51,53−57] and of the scaling exponent (α = 0.29 − 1.06)[49,57−61] depending on the material type, whether it is a monolayer or a multilayer, substrate, and contact material. Most relevant, in phototransistors of monolayer TMDCs on silicon oxide, the scaling was found to depend on the doping level, as controlled through the electrostatic gate.[49,58] At low doping, the scaling is linear and becomes sublinear at higher doping, falling to α = 0.7.[57,58] Though the exact mechanism is still under debate, this change in scaling is often attributed to the gate-dependent screening of trap states present in the MoS_2 or WSe_2 channel or at the interface between the channel and substrate.[51,52] Importantly, the crumpled devices have no gate, so the charge density is determined purely from the intrinsic doping due to material quality, environmental interaction, and residual strain. As a result, the magnitude of the scaling informs on the doping state of the phototransistor channel and reveals that WSe_2 is doped to near a band edge.

In Figure 4, we examine the spatially resolved photocurrent. Figure 4a,b shows photocurrent maps at 0 and 1 V drain bias, respectively, at 100 μW laser power of the same phototransistor studied in Figure 3. At zero bias, the phototransistor displays an asymmetric photocurrent isolated to the graphene contacts with a responsivity of up to 0.08 μA/W. At 1 V bias, the photocurrent is distributed through the monolayer WSe_2 channel with a responsivity of 1.3 μA/W, a magnitude consistent with the power scaling measured in Figure 3. The voltage-dependent and asymmetric behavior at zero bias is comparable to that of Cr/Au (Ti/Au) contacted WSe_2 (MoS_2) phototransistors on a SiO_2/Si substrate[62] and is typically due to separation of excitons at the Schottky barrier at the contacts. The sign of the current gives the relative work function and direction of band bending at the graphene−WSe_2 junctions.

Figure 4c,d shows additional photocurrent maps under bias of a second phototransistor before and after crumpling under 15% compression. All the photocurrent maps display spatial fluctuations in the magnitude of the current along the channel of about a factor of 2, even before crumpling, suggesting that the inhomogeneity primarily comes from sources unrelated to strain, such as multilayer patches or inhomogeneous contact resistance. Meanwhile, Figure 4c,d shows that, after crumpling, the active area of the phototransistor shrinks and the photoresponsivity increases by about 20% on average. Previous studies on flat, strained phototransistors have shown that the strain-induced band gap modulations discussed above lead to effective changes in photoresponsivity by 2−3 orders of magnitude where the strain ranges from −1.44 to 0.48%.[46] Meanwhile, a biaxial crumpling of >250% in graphene increases the optical extinction by a factor of 12.5 over flat graphene[18] due to densification per unit area. Taken together, these factors easily explain the changes in signal magnitude. In this context, the small changes in the photoresponse observed in the 15% biaxially crumpled device show that the residual strain after crumpling and densification per unit area are not enough to dramatically alter the device behavior.

Figure 4e,f shows the band diagrams of the crumpled phototransistor under 0 and 1 V drain bias as inferred from the global and local photocurrent measurements. External laser excitation generates an electron−hole pair in the WSe_2 layer, which travels in the direction of the electrical field present. In Figure 4e, the electrons and holes follow the direction of the built-in electrical field near the graphene−WSe_2 junctions giving opposing photocurrent signals at the junctions. In Figure 4f, the electron and hole travel according to the direction of the externally applied electrical field. In both situations, the spatial fluctuations in the band gap and doping are large enough to alter but not dominate the device behavior. These results indicate that while the large deformations lead to a spatially inhomogeneous response, crumpled 2D heterostructures maintain the functionality of their flat analogs, with potential for strain resilient electronics.

CONCLUSIONS

In summary, we demonstrated a new concept of devices based on crumpled van der Waals heterostructures. We investigate the crumpling morphology of the heterostructure and the device behavior of a phototransistor based on a graphene−WSe_2 heterostructure. The 2D membranes relieve the applied compressive stress through delamination from the substrate, and the interface between the 2D layers is maintained through large deformations. Yet, because the stress in the membrane is relieved through the crumpling, the heterostructure maintains good electronic performance under strains large enough to fracture or dramatically alter the electronic structure of a flat device. Next steps include resolving how heterostructures will behave under dynamically variable strains, and how reversible the crumpling process is, and applying the same concept to more complex heterostructures, such as logic devices like transistors. There have been hundreds of demonstrations of devices based on 2D heterostructures, so this device concept could be generalized, leading to the potential for high-mobility, yet deformable integrated circuitry for wearable electronics.

ASSOCIATED CONTENT

Supporting Information

The Supporting Information is available free of charge at https://pubs.acs.org/doi/10.1021/acsami.0c10787.

Details on sample preparation, inducing and controlling uniaxial and biaxial compression, effect of the Poisson ratio of the substrate, comparison of different 2D materials and substrates on the morphology of uniaxially crumpled structures, optical spectroscopy of flat and crumpled materials, and photocurrent measurement (PDF)

AUTHOR INFORMATION

Corresponding Author

Arend M. van der Zande − *Department of Mechanical Science and Engineering and Materials Research Laboratory, University of Illinois at Urbana-Champaign, Urbana, Illinois 61801, United States;* orcid.org/0000-0001-5104-9646; Email: arendv@illinois.edu

Authors

M. Abir Hossain − *Department of Mechanical Science and Engineering, University of Illinois at Urbana-Champaign, Urbana, Illinois 61801, United States;* orcid.org/0000-0003-1606-5960

Jaehyung Yu − *Department of Mechanical Science and Engineering, University of Illinois at Urbana-Champaign,*

https://dx.doi.org/10.1021/acsami.0c10787
ACS Appl. Mater. Interfaces XXXX, XXX, XXX−XXX

Urbana, Illinois 61801, United States; orcid.org/0000-0002-9925-2309

Complete contact information is available at: https://pubs.acs.org/10.1021/acsami.0c10787

Author Contributions

A.M.v.d.Z. and M.A.H. conceived the idea and designed the experiments. M.A.H. and J.Y. conducted material growth and performed atomic force microscopy imaging. M.A.H. performed device fabrication, optoelectronic measurements, and analyzed the data. All authors contributed to writing the manuscript.

Notes

The authors declare no competing financial interest.

■ ACKNOWLEDGMENTS

This research was solely supported by the National Science Foundation MRSEC program under NSF Award Number DMR-1720633. This work was carried out in the Material Research Laboratory Central Facilities and the Micro and Nano Technology Laboratory, and the iMRSEC shared facilities DMR-1720633. We thank Jangyup Son, SunPhil Kim, Paolo Ferrari, Juyoung Leem, and SungWoo Nam for helpful discussions.

■ REFERENCES

(1) Rogers, J. A.; Someya, T.; Huang, Y. Materials and Mechanics for Stretchable Electronics. *Science* **2010**, *327*, 1603−1607.

(2) Dodabalapur, A. Organic and Polymer Transistors for Electronics. *Mater. Today* **2006**, *9*, 24−30.

(3) Nathan, A.; Ahnood, A.; Cole, M. T.; Lee, S.; Suzuki, Y.; Hiralal, P.; Bonaccorso, F.; Hasan, T.; Garcia-Gancedo, L.; Dyadyusha, A.; Haque, S.; Andrew, P.; Hofmann, S.; Moultrie, J.; Chu, D.; Flewitt, A. J.; Ferrari, A. C.; Kelly, M. J.; Robertson, J.; Amaratunga, G. A. J.; Milne, W. I. Flexible Electronics: The Next Ubiquitous Platform. *Proceedings of the IEEE* **2012**, 1486−1517.

(4) Akinwande, D.; Brennan, C. J.; Bunch, J. S.; Egberts, P.; Felts, J. R.; Gao, H.; Huang, R.; Kim, J.-S.; Li, T.; Li, Y.; Liechti, K. M.; Lu, N.; Park, H. S.; Reed, E. J.; Wang, P.; Yakobson, B. I.; Zhang, T.; Zhang, Y.-W.; Zhou, Y.; Zhu, Y. A Review on Mechanics and Mechanical Properties of 2D Materials—Graphene and Beyond. *Extrem. Mech. Lett.* **2017**, *13*, 42−77.

(5) Kim, J. H.; Jeong, J. H.; Kim, N.; Joshi, R.; Lee, G. H. Mechanical Properties of Two-Dimensional Materials and Their Applications. *J. Phys. D: Appl. Phys.* **2019**, *52*, No. 083001.

(6) Geim, A. K.; Grigorieva, I. V. Van Der Waals Heterostructures. *Nature* **2013**, *499*, 419−425.

(7) Liu, Y.; Weiss, N. O.; Duan, X.; Cheng, H.-C.; Huang, Y.; Duan, X. Van Der Waals Heterostructures and Devices. *Nat. Rev. Mater.* **2016**, *1* (9), 16042.

(8) Zultak, J.; Magorrian, S. J.; Koperski, M.; Garner, A.; Hamer, M. J.; Tóvári, E.; Novoselov, K. S.; Zhukov, A. A.; Zou, Y.; Wilson, N. R.; Haigh, S. J.; Kretinin, A. V.; Fal'ko, V. I.; Gorbachev, R. Ultra-Thin van Der Waals Crystals as Semiconductor Quantum Wells. *Nat. Commun.* **2020**, *11*, 1−6.

(9) Zhang, Z.-Z.; Song, X.-X.; Luo, G.; Deng, G.-W.; Mosallanejad, V.; Taniguchi, T.; Watanabe, K.; Li, H.-O.; Cao, G.; Guo, G.-C.; Nori, F.; Guo, G.-P. Electrotunable Artificial Molecules Based on van Der Waals Heterostructures. *Sci. Adv.* **2017**, *3*, No. e1701699.

(10) Hamer, M.; Tóvári, E.; Zhu, M.; Thompson, M. D.; Mayorov, A.; Prance, J.; Lee, Y.; Haley, R. P.; Kudrynskyi, Z. R.; Patanè, A.; Terry, D.; Kovalyuk, Z. D.; Ensslin, K.; Kretinin, A. V.; Geim, A.; Gorbachev, R. Gate-Defined Quantum Confinement in InSe-Based van Der Waals Heterostructures. *Nano Lett.* **2018**, *18*, 3950−3955.

(11) Bunch, J. S.; Van Der Zande, A. M.; Verbridge, S. S.; Frank, I. W.; Tanenbaum, D. M.; Parpia, J. M.; Craighead, H. G.; McEuen, P. L. Electromechanical Resonators from Graphene Sheets. *Science* **2007**, *315*, 490−493.

(12) Van Der Zande, A. M.; Barton, R. A.; Alden, J. S.; Ruiz-Vargas, C. S.; Whitney, W. S.; Pham, P. H. Q.; Park, J.; Parpia, J. M.; Craighead, H. G.; McEuen, P. L. Large-Scale Arrays of Single-Layer Graphene Resonators. *Nano Lett.* **2010**, *10*, 4869−4873.

(13) Kim, S.; Yu, J.; Van Der Zande, A. M. Nano-Electromechanical Drumhead Resonators from Two-Dimensional Material Bimorphs. *Nano Lett.* **2018**, *18*, 6686−6695.

(14) Lee, G.-H.; Yu, Y.-J.; Cui, X.; Petrone, N.; Lee, C.-H.; Choi, M. S.; Lee, D.-Y.; Lee, C.; Yoo, W. J.; Watanabe, K.; Taniguchi, T.; Nuckolls, C.; Kim, P.; Hone, J. Flexible and Transparent MoS_2 Field-Effect Transistors on Hexagonal Boron Nitride-Graphene Heterostructures. *ACS Nano* **2013**, *7*, 7931−7936.

(15) Georgiou, T.; Jalil, R.; Belle, B. D.; Britnell, L.; Gorbachev, R. V.; Morozov, S. V.; Kim, Y. J.; Gholinia, A.; Haigh, S. J.; Makarovsky, O.; Eaves, L.; Ponomarenko, L. A.; Geim, A. K.; Novoselov, K. S.; Mishchenko, A. Vertical Field-Effect Transistor Based on Graphene-WS_2 Heterostructures for Flexible and Transparent Electronics. *Nat. Nanotechnol.* **2013**, *8*, 100−103.

(16) Petrone, N.; Meric, I.; Hone, J.; Shepard, K. L. Graphene Field-Effect Transistors with Gigahertz-Frequency Power Gain on Flexible Substrates. *Nano Lett.* **2013**, *13*, 121−125.

(17) Akinwande, D.; Petrone, N.; Hone, J. Two-Dimensional Flexible Nanoelectronics. *Nat. Commun.* **2014**, *5*, 1.

(18) Kang, P.; Wang, M. C.; Knapp, P. M.; Nam, S. Crumpled Graphene Photodetector with Enhanced, Strain-Tunable, and Wavelength-Selective Photoresponsivity. *Adv. Mater.* **2016**, *28*, 4639−4645.

(19) Deng, S.; Berry, V. Wrinkled, Rippled and Crumpled Graphene: An Overview of Formation Mechanism, Electronic Properties, and Applications. *Mater. Today* **2016**, *19*, 197−212.

(20) Chen, W.; Gui, X.; Yang, L.; Zhu, H.; Tang, Z. Wrinkling of Two-Dimensional Materials: Methods Properties and Applications. *Nanoscale Horiz.* **2019**, *4*, 291−320.

(21) Yu, J.; Kim, S.; Ertekin, E.; Van Der Zande, A. M. Material-Dependent Evolution of Mechanical Folding Instabilities in Two-Dimensional Atomic Membranes. *ACS Appl. Mater. Interfaces* **2020**, 10801.

(22) Wang, Y.; Yang, R.; Shi, Z.; Zhang, L.; Shi, D.; Wang, E.; Zhang, G. Super-Elastic Graphene Ripples for Flexible Strain Sensors. *ACS Nano* **2011**, *5*, 3645−3650.

(23) Yang, S.; Wang, C.; Sahin, H.; Chen, H.; Li, Y.; Li, S.-S.; Suslu, A.; Peeters, F. M.; Liu, Q.; Li, J.; Tongay, S. Tuning the Optical, Magnetic, and Electrical Properties of $ReSe_2$ by Nanoscale Strain Engineering. *Nano Lett.* **2015**, *15*, 1660−1666.

(24) Lim, S.; Luan, H.; Zhao, S.; Lee, Y.; Zhang, Y.; Huang, Y.; Rogers, J. A.; Ahn, J.-H. Assembly of Foldable 3D Microstructures Using Graphene Hinges. *Adv. Mater.* **2020**, *32*, 1−8.

(25) Zang, J.; Cao, C.; Feng, Y.; Liu, J.; Zhao, X. Stretchable and High-Performance Supercapacitors with Crumpled Graphene Papers. *Sci. Rep.* **2014**, *4*, 1.

(26) Zang, J.; Ryu, S.; Pugno, N.; Wang, Q.; Tu, Q.; Buehler, M. J.; Zhao, X. Multifunctionality and Control of the Crumpling and Unfolding of Large-Area Graphene. *Nat. Mater.* **2013**, *12*, 321−325.

(27) Hwang, M. T.; Heiranian, M.; Kim, Y.; You, S.; Leem, J.; Taqieddin, A.; Faramarzi, V.; Jing, Y.; Park, I.; van der Zande, A. M.; Nam, S.; Aluru, N. R.; Bashir, R. Ultrasensitive Detection of Nucleic Acids Using Deformed Graphene Channel Field Effect Biosensors. *Nat. Commun.* **2020**, *11*, 1543.

(28) Hossain, M. A.; Zhang, Y.; van der Zande, A. M. Strain engineering photonic properties in monolayer semiconductors through mechanically-reconfigurable wrinkling. In *Physical Chemistry of Semiconductor Materials and Interfaces XIX, Proceedings of SPIE*, Aug 20, 2020, Nielsen, C., Congreve, D., Eds.; SPIE: 2020; 1146404, 1−7, .

(29) Han, E.; Yu, J.; Annevelink, E.; Son, J.; Kang, D. A.; Watanabe, K.; Taniguchi, T.; Ertekin, E.; Huang, P. Y.; van der Zande, A. M. Ultrasoft Slip-Mediated Bending in Few-Layer Graphene. *Nat. Mater.* **2020**, *19*, 305−309.

(30) Thomas, A. V.; Andow, B. C.; Suresh, S.; Eksik, O.; Yin, J.; Dyson, A. H.; Koratkar, N. Controlled Crumpling of Graphene Oxide Films for Tunable Optical Transmittance. *Adv. Mater.* **2015**, *27*, 3256−3265.
(31) Rhee, D.; Paci, J. T.; Deng, S.; Lee, W. K.; Schatz, G. C.; Odom, T. W. Soft Skin Layers Enable Area-Specific, Multiscale Graphene Wrinkles with Switchable Orientations. *ACS Nano* **2020**, *14*, 166−174.
(32) Zhu, W.; Low, T.; Perebeinos, V.; Bol, A. A.; Zhu, Y.; Yan, H.; Tersoff, J.; Avouris, P. Structure and Electronic Transport in Graphene Wrinkles. *Nano Lett.* **2012**, *12*, 3431−3436.
(33) Kim, K.; Lee, Z.; Malone, B. D.; Chan, K. T.; Alemán, B.; Regan, W.; Gannett, W.; Crommie, M. F.; Cohen, M. L.; Zettl, A. Multiply Folded Graphene. *Phys. Rev. B* **2011**, *83*, 245433.
(34) Zhang, Y.; Wei, N.; Zhao, J.; Gong, Y.; Rabczuk, T. Quasi-Analytical Solution for the Stable System of the Multi-Layer Folded Graphene Wrinkles. *J. Appl. Phys.* **2013**, *114*, No. 063511.
(35) Brennan, C. J.; Nguyen, J.; Yu, E. T.; Lu, N. Interface Adhesion between 2D Materials and Elastomers Measured by Buckle Delaminations. *Adv. Mater. Interfaces* **2015**, *2*, 1500176.
(36) Khestanova, E.; Guinea, F.; Fumagalli, L.; Geim, A. K.; Grigorieva, I. V. Universal Shape and Pressure inside Bubbles Appearing in van Der Waals Heterostructures. *Nat. Commun.* **2016**, *7*, 1−10.
(37) Sanchez, D. A.; Dai, Z.; Wang, P.; Cantu-Chavez, A.; Brennan, C. J.; Huang, R.; Lu, N. Mechanics of Spontaneously Formed Nanoblisters Trapped by Transferred 2D Crystals. *Proc. Natl. Acad. Sci. U. S. A.* **2018**, *115*, 7884−7889.
(38) Dean, C. R.; Young, A. F.; Meric, I.; Lee, C.; Wang, L.; Sorgenfrei, S.; Watanabe, K.; Taniguchi, T.; Kim, P.; Shepard, K. L.; Hone, J. Boron Nitride Substrates for High-Quality Graphene Electronics. *Nat. Nanotechnol.* **2010**, *5*, 722−726.
(39) Scharfenberg, S.; Rocklin, D. Z.; Chialvo, C.; Weaver, R. L.; Goldbart, P. M.; Mason, N. Probing the Mechanical Properties of Graphene Using a Corrugated Elastic Substrate. *Appl. Phys. Lett.* **2011**, *98*, No. 091908.
(40) Zhang, Z.; Li, T. Determining Graphene Adhesion via Substrate-Regulated Morphology of Graphene. *J. Appl. Phys.* **2011**, *110*, No. 083526.
(41) Zhu, L.; Chen, X. Delamination-Based Measurement and Prediction of the Adhesion Energy of Thin Film/Substrate Interfaces. *J. Eng. Mater. Technol. Trans.* **2017**, *139*, No. 021021.
(42) Liu, K.; Yan, Q.; Chen, M.; Fan, W.; Sun, Y.; Suh, J.; Fu, D.; Lee, S.; Zhou, J.; Tongay, S.; Ji, J.; Neaton, J. B.; Wu, J. Elastic Properties of Chemical-Vapor-Deposited Monolayer MoS_2 , WS_2 , and Their Bilayer Heterostructures. *Nano Lett.* **2014**, *14*, 5097−5103.
(43) He, K.; Poole, C.; Mak, K. F.; Shan, J. Experimental Demonstration of Continuous Electronic Structure Tuning via Strain in Atomically Thin MoS_2. *Nano Lett.* **2013**, *13*, 2931−2936.
(44) Conley, H. J.; Wang, B.; Ziegler, J. I.; Haglund, R. F., Jr.; Pantelides, S. T.; Bolotin, K. I. Bandgap Engineering of Strained Monolayer and Bilayer MoS_2. *Nano Lett.* **2013**, *13*, 3626−3630.
(45) Aslan, O. B.; Deng, M.; Heinz, T. F. Strain Tuning of Excitons in Monolayer WSe_2. *Phys. Rev. B* **2018**, *98*, 115308.
(46) Gant, P.; Huang, P.; Pérez de Lara, D.; Guo, D.; Frisenda, R.; Castellanos-Gomez, A. A Strain Tunable Single-Layer MoS_2 Photodetector. *Mater. Today* **2019**, *27*, 8−13.
(47) Lloyd, D.; Liu, X.; Christopher, J. W.; Cantley, L.; Wadehra, A.; Kim, B. L.; Goldberg, B. B.; Swan, A. K.; Bunch, J. S. Band Gap Engineering with Ultralarge Biaxial Strains in Suspended Monolayer MoS2. *Nano Lett.* **2016**, *16*, 5836−5841.
(48) Castellanos-Gomez, A.; Roldán, R.; Cappelluti, E.; Buscema, M.; Guinea, F.; Van Der Zant, H. S. J.; Steele, G. A. Local Strain Engineering in Atomically Thin MoS2. *Nano Lett.* **2013**, *13*, 5361−5366.
(49) Tan, H.; Fan, Y.; Zhou, Y.; Chen, Q.; Xu, W.; Warner, J. H. Ultrathin 2D Photodetectors Utilizing Chemical Vapor Deposition Grown WS_2 with Graphene Electrodes. *ACS Nano* **2016**, *10*, 7866−7873.
(50) Sze, S. M.; Ng, K. K. *Physics of Semiconductor Devices*; John Wiley & Sons, Inc.: Hoboken, NJ, USA, 2006.
(51) Lopez-Sanchez, O.; Lembke, D.; Kayci, M.; Radenovic, A.; Kis, A. Ultrasensitive Photodetectors Based on Monolayer MoS_2. *Nat. Nanotechnol.* **2013**, *8*, 497−501.
(52) Furchi, M. M.; Polyushkin, D. K.; Pospischil, A.; Mueller, T. Mechanisms of Photoconductivity in Atomically Thin MoS_2. *Nano Lett.* **2014**, *14*, 6165−6170.
(53) Chen, J.; Liu, B.; Liu, Y.; Tang, W.; Nai, C. T.; Li, L.; Zheng, J.; Gao, L.; Zheng, Y.; Shin, H. S.; Jeong, H. Y.; Loh, K. P. Chemical Vapor Deposition of Large-Sized Hexagonal WSe_2 Crystals on Dielectric Substrates. *Adv. Mater.* **2015**, *27*, 6722−6727.
(54) Zhang, W.; Chiu, M.-H.; Chen, C.-H.; Chen, W.; Li, L.-J.; Wee, A. T. S. Role of Metal Contacts in High-Performance Phototransistors Based on WSe_2 Monolayers. *ACS Nano* **2014**, *8*, 8653−8661.
(55) Perea-López, N.; Lin, Z.; Pradhan, N. R.; Iñiguez-Rábago, A.; Elías, A. L.; McCreary, A.; Lou, J.; Ajayan, P. M.; Terrones, H.; Balicas, L.; Terrones, M. CVD-Grown Monolayered MoS_2 as an Effective Photosensor Operating at Low-Voltage. *2D Mater.* **2014**, *1* (1), 11004.
(56) Zhang, W.; Huang, J. K.; Chen, C. H.; Chang, Y. H.; Cheng, Y. J.; Li, L. J. High-Gain Phototransistors Based on a CVD MoS_2 Monolayer. *Adv. Mater.* **2013**, *25*, 3456−3461.
(57) Yin, Z.; Li, H.; Li, H.; Jiang, L.; Shi, Y.; Sun, Y.; Lu, G.; Zhang, Q.; Chen, X.; Zhang, H. Single-Layer MoS_2 Phototransistors. *ACS Nano* **2012**, *6*, 74−80.
(58) Wu, G.; Wang, X.; Chen, Y.; Wang, Z.; Shen, H.; Lin, T.; Hu, W.; Wang, J.; Zhang, S.; Meng, X.; Chu, J. Ultrahigh Photoresponsivity MoS_2 Photodetector with Tunable Photocurrent Generation Mechanism. *Nanotechnology* **2018**, *29*, 485204.
(59) Huang, J.; Yang, L.; Liu, D.; Chen, J.; Fu, Q.; Xiong, Y.; Lin, F.; Xiang, B. Large-Area Synthesis of Monolayer WSe_2 on a SiO_2/Si Substrate and Its Device Applications. *Nanoscale* **2015**, *7*, 4193−4198.
(60) Zheng, Z.; Zhang, T.; Yao, J.; Zhang, Y.; Xu, J.; Yang, G. Flexible, Transparent and Ultra-Broadband Photodetector Based on Large-Area WSe_2 Film for Wearable Devices. *Nanotechnology* **2016**, *27*, 225501.
(61) Wang, T.; Andrews, K.; Bowman, A.; Hong, T.; Koehler, M.; Yan, J.; Mandrus, D.; Zhou, Z.; Xu, Y.-Q. High-Performance WSe_2 Phototransistors with 2D/2D Ohmic Contacts. *Nano Lett.* **2018**, *18*, 2766−2771.
(62) Yi, Y.; Wu, C.; Liu, H.; Zeng, J.; He, H.; Wang, J. A Study of Lateral Schottky Contacts in WSe_2 and MoS_2 Field Effect Transistors Using Scanning Photocurrent Microscopy. *Nanoscale* **2015**, *7*, 15711−15718.

https://dx.doi.org/10.1021/acsami.0c10787
ACS Appl. Mater. Interfaces XXXX, XXX, XXX−XXX